

The Synthesis, Crystal Structure, and Magnetic Properties of Perovskites $Ba_3Ln_2MO_9$ (Ln = Lanthanides; M = Mo, W)

Shigeaki Oyama, Yoshihiro Doi, Yukio Hinatsu,* and Yoshinobu Ishii[1]

Division of Chemistry, Graduate School of Science, Hokkaido University, Sapporo 060-0810

[1]Japan Atomic Energy Research Institute, Tokai-mura, Ibaraki 319-1195

Received February 18, 2004; E-mail: hinatsu@sci.hokudai.ac.jp

The synthesis, crystal structure, and magnetic properties of quaternary oxides $Ba_3Ln_2MO_9$ (Ln = Y, Sm–Gd, Dy–Lu for M = Mo; Ln = Y, Sm–Lu for M = W) are reported. Their powder X-ray diffraction measurements and Rietveld analysis showed that they have a "disordered" perovskite structure, i.e., $BaLn_{2/3}M_{1/3}O_3$ except for $Ba_3Tb_2WO_9$, and that their structures are monoclinic with space group $I2/c$ (Ln = Y, Sm–Gd, Dy–Yb for M = Mo; Ln = Y, Sm–Lu for M = W) or cubic with space group $Pm\bar{3}m$ (Ln = Lu for M = Mo). Powder neutron diffraction measurements showed that $Ba_3Tb_2WO_9$ has an ordered perovskite structure and is monoclinic with space group $P2_1/n$. Magnetic susceptibility measurements showed that all the $Ba_3Ln_2MO_9$ compounds are paramagnetic down to 1.8 K. The Tb ions of $Ba_3Tb_2WO_9$ are in the mixed valence state (+3, +4). Through ^{151}Eu Mössbauer measurements on $Ba_3Eu_2MoO_9$ and $Ba_3Eu_2WO_9$, it was found that the Eu ion is in the trivalent state, and that the symmetry of the Eu site is distorted from the octahedral symmetry.

It is well known that the most stable oxidation state of lanthanide (Ln) ions is trivalent, and that the electronic configuration of Ln^{3+} ions is [Xe]$4f^n$ ([Xe]: xenon electronic core). The magnetic properties of lanthanide ions are fascinating in their systematic variety and intelligible complexity. Their magnetic properties are determined by the behavior of unpaired 4f electrons. These are highly localized electrons, and the shielding by the surrounding 5s and 5p electrons in the outer shell makes the magnetic interactions between 4f electrons in solids very weak. In fact, many of the lanthanide oxides order magnetically below 4 K. One of the most challenging problems in the modern chemistry of lanthanide compounds is to find a compound in which strong magnetic interactions between 4f electrons exist, which gives rise to a long-range magnetic order at relatively high temperatures. We have been focusing our attention on perovskite-type compounds containing lanthanide ions.

The perovskite-type oxides have the general formula ABO_3, where A represents a large metal cation and B represents a small one. The perovskite structure can be described as a framework of corner-shared BO_6 octahedra which contains A cations at 12-coordinate sites. The lanthanide ion is relatively large, and tends to adopt a high coordination number. Therefore, the lanthanide ion usually sits at the A site of the perovskite oxide ABO_3. By selecting large alkaline earth elements such as Sr and Ba as the A site atoms, one finds that lanthanides occupy the 6-coordinate B sites. The perovskite-type oxides have some flexibility in their chemical composition and crystal structure. Combining many kinds of ions and control of their crystal structures are possible.

In "ordered" perovskite-type oxides $A_2B'B''O_6$ or $A_3B'B''_2O_9$, two kinds of cations at the B sites, B′ and B″, are regularly ordered, i.e., 1:1 or 1:2 arrangement of B′ and B″ ions has been observed over the six-coordinate B sites.[1,2] Since the B site ions normally determine the physical properties of the perovskites, the ordered perovskite-type oxides can show a variety of physical properties reflecting the nature of the constituent B′ and B″ cations. So far, we have studied the preparation, crystal structure, and magnetic properties of ordered perovskite-type oxides containing lanthanides, Ba_2LnMO_6 (M = Nb, Ta, Ru, Ir).[3–6]

Now, our focus has turned to the $A_3B'B''_2O_9$ compounds. There exist three types of B′ and B″ arrangements concerning the B-site cations. When different B′ and B″ cations are situated on crystallographically distinct sites, 1:2 B-site cation ordering occurs. This type of order has been reported for many $A_3B'B''_2O_9$ compounds. We have found this type of order in perovskite-type oxides containing lanthanides and ruthenium ($Ba_3LnRu_2O_9$), and observed peculiar magnetic properties at low temperatures.[7] It should be noted that not all the compounds in which the B′:B″ ratio is 1:2 are genuine examples of 1:2 ordering. In some instances the real order is 1:1, as the B″ cations are distributed over both B sites, i.e., the ordering is such that one of the B sites is fully occupied by B″, whereas the other contains 2/3B′ and 1/3B″ with a random distribution, and therefore the chemical formula should be described as $A_2(B'_{2/3}B''_{1/3})B''O_6$. The third case is that B′ and B″ cations are disordered at the B site of the perovskite ABO_3.

In this paper, we will study the crystal structure and magnetic properties of perovskite-type oxides $Ba_3Ln_2MO_9$ (M = Mo, W). Because of the large difference in the ionic radius between Ln and Mo or W cations, a structural ordering of these cations should be present. The valence states of the Mo and W cations in $Ba_3Ln_2MO_9$ are expected to be hexavalent, and their electronic configurations should be [Kr]$4d^0$ and [Xe]$4f^{14}$ ([Kr]: krypton electronic core; [Xe]: xenon electronic core), respectively. The magnetic properties of compounds $Ba_3Ln_2MO_9$ will

Published on the web July 9, 2004; DOI 10.1246/bcsj.77.1359

then depend only on the magnetic behavior of the Ln ions. Therefore, this system is appropriate for studying the magnetic properties of f-electrons in the B site of perovskites.

Experimental

Polycrystalline samples of $Ba_3Ln_2MO_9$ were prepared by a standard solid state reaction. As starting materials, barium carbonate ($BaCO_3$), lanthanide sesquioxide (Ln_2O_3) (Ln = Y, La, Nd, Sm–Gd, Dy–Lu), and molybdenum oxide (MoO_3) or tungsten oxide (WO_3) were used. For the cases of Ce, Pr, and Tb, CeO_2, Pr_6O_{11}, and Tb_4O_7 were used. These reagents were weighed in appropriate metal ratios and ground together in an agate mortar. The mixtures were pressed into pellets and then calcined in air at 1173 K for 12 h. After being cooled to room temperature, the pellets were reground, repressed, and heated in air at 1623–1773 K for several days with intermediate regrinding and repelletizing.

Powder X-ray diffraction (XRD) patterns were measured with Cu Kα radiation on a MultiFlex diffractometer (Rigaku, Japan). XRD data were collected by step scanning over the range $10^\circ \leq 2\theta \leq 120^\circ$ in increments of 0.02°. The structure refinements were carried out by Rietveld analysis for the XRD data with the RIETAN2000 program.[8]

A powder neutron diffraction pattern for $Ba_3Tb_2WO_9$ was measured with a high-resolution powder diffractometer (HRPD) at the JRR-3M Reactor (Japan Atomic Energy Research Institute), with a Ge(331) monochromator. The measurement was made at room temperature in the range $4^\circ \leq 2\theta \leq 120^\circ$ at intervals of 0.1° with a wavelength of 1.82301 Å.

Magnetic susceptibility measurements were performed using a SQUID magnetometer (Quantum Design MPMS). A susceptibility–temperature curve was measured under both the ZFC (zero-field-cooled) and the FC (field-cooled) conditions. Magnetic susceptibilities for two series of $Ba_3Ln_2MoO_9$ and $Ba_3Ln_2WO_9$ were measured in a magnetic field of 0.01 T or 0.1 T over the temperature range between 1.8 and 300 K.

The ^{151}Eu Mössbauer spectrum was measured with a conventional transmissional Mössbauer spectrometer VT-6000 (Laborato-

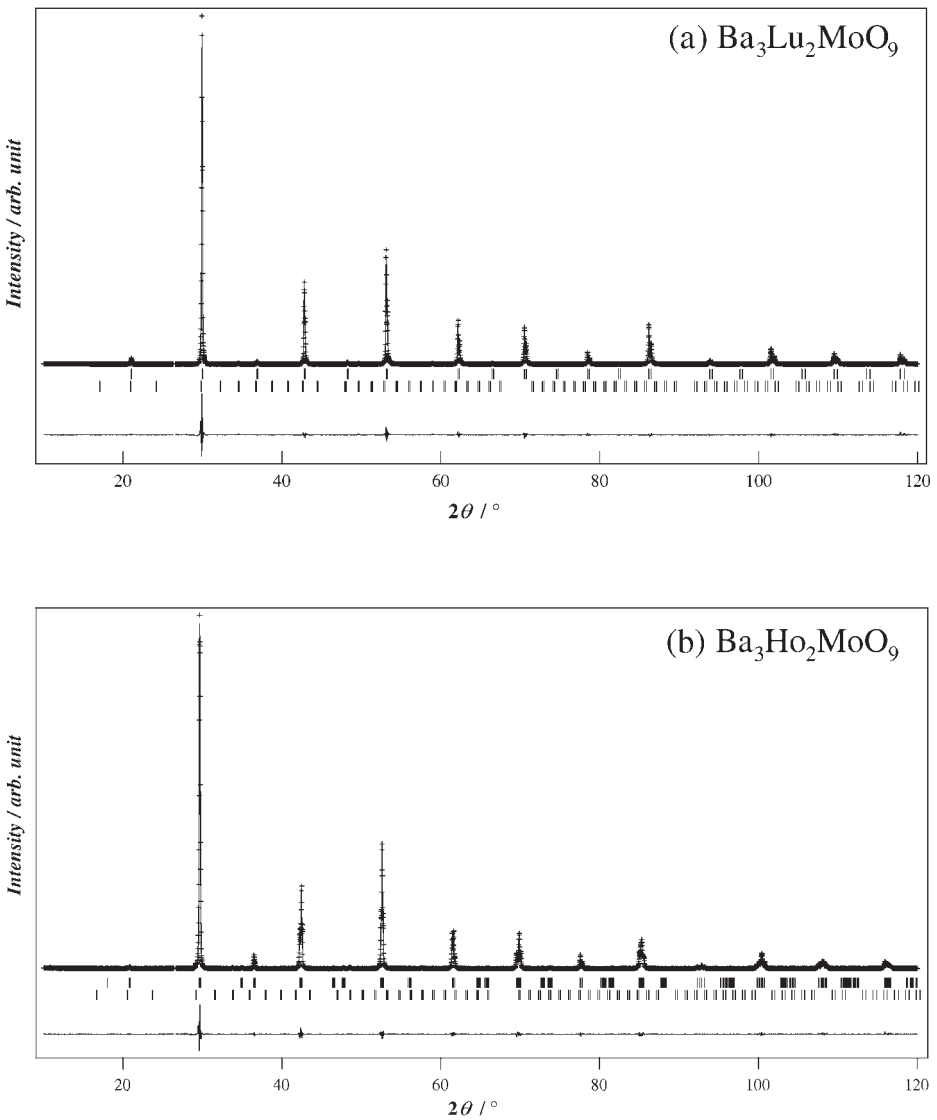

Fig. 1. X-ray diffraction profiles for (a) $Ba_3Lu_2MoO_9$ and (b) $Ba_3Ho_2MoO_9$. The calculated and observed diffraction profiles are shown on the top as a solid line and cross markers, respectively. The vertical marks show positions calculated from Bragg reflections. The bottom traces are plots of the difference between calculated and observed intensities.

ry Equipment Co.) in the constant acceleration mode. The spectrometer was calibrated with a spectrum of α-Fe at room temperature. A $^{151}SmF_3$ radiation source (1.85 GBq) was used and γ-rays were detected with a NaI scintillation counter. EuF_3 was used as a reference standard for the chemical isomer shift. The average surface density of the sample was 15.0 mg (Eu) cm^{-2}.

Results and Discussion

Synthesis and Crystal Structures. The results of the X-ray diffraction measurements show that both the $Ba_3Ln_2MoO_9$ (Ln = Y, Sm–Gd, Dy–Lu) and $Ba_3Ln_2WO_9$ (Ln = Y, Sm–Lu) compounds have a perovskite structure. In these compounds, some impurities such as Ln_2O_3 and scheelite-like $BaMoO_4$[9] were found. Since their ratios are below 0.5–2 mol%, such impurities do not have an influence on the magnetic properties of the above compounds. On the other hand, a single phase compound was not formed for $Ba_3Ln_2MO_9$ (Ln = La, Ce, Pr, Nd; M = Mo, W) or $Ba_3Tb_2MoO_9$ because the size of Ln^{3+} ions (Ln = La–Nd) is too large for the B-site cations of the perovskite ABO_3. The X-ray diffraction patterns for $Ba_3Lu_2MoO_9$ were indexed with a cubic unit cell, whereas $Ba_3Ln_2MoO_9$ (Ln = Y, Sm–Gd, Dy–Yb) and $Ba_3Ln_2WO_9$ (Ln = Y, Sm–Lu) were monoclinically distorted. Figure 1 shows the X-ray diffraction profiles for $Ba_3Lu_2MoO_9$ and $Ba_3Ho_2MoO_9$. The diffraction reflection at $2\theta \approx 18^\circ$ was not observed for any compound except for $Ba_3Tb_2WO_9$. The absence of this reflection indicates that the B site ions are disordered. Since these compounds have a disordered perovskite-type structure, their structures are refined by applying the space group $Pm\bar{3}m$ (No. 221, $a_p \times a_p \times a_p$) for the $Ba_3Lu_2MoO_9$ compound and $I2/c$ (No. 15, $\sqrt{2}a_p \times \sqrt{2}a_p \times 2a_p$) for the other compounds.[10] Figure 2 shows the X-ray diffraction profiles for $Ba_3Tb_2WO_9$. A reflection at $2\theta \approx 18^\circ$ was observed only for $Ba_3Tb_2WO_9$. The presence of this reflection indicates that there exists 1:1 ordered arrangement between the B site ions. Its structure was refined by applying the space group $P2_1/n$ (No. 14, $\sqrt{2}a_p \times \sqrt{2}a_p \times 2a_p$). This is because the reliability factors obtained by applying the space group $P2_1/n$ are the smallest and were the most reliable result after applying other possible space groups. The unit cell parameters and the reliability factors for all compounds are listed in Table 1. The crystallographic data for $Ba_3Lu_2MoO_9$ and $Ba_3Ho_2MoO_9$ are shown in Table 2.

To discuss the stability of the perovskite-type compounds ABO_3, Goldshmidt introduced the tolerance factor (t), defined by $t = (r_A + r_O)/\sqrt{2}(r_B + r_O)$, where r_A, r_B, and r_O are the radii of the A and B metal ions and oxygen ions, respectively. For $A_3B_2B'O_9$ compounds, it is modified by $t = (r_A + r_O)/\sqrt{2}\{(2/3r_B + 1/3r_{B'}) + r_O\}$, where r_B and $r_{B'}$ are the radii of the B and B′ metal ions, respectively. For tolerance factor less than unity, the perovskite structure distorts from the ideal cubic symmetry. The Ln^{3+} ionic radius decreases with the increasing atomic number of lanthanide elements. Therefore, the tolerance factors (t) of $Ba_3Ln_2MoO_9$ ($Ba_3Ln_2WO_9$) increase from $t = 0.950$ ($t = 0.949$) for $Ba_3Sm_2MoO_9$ ($Ba_3Sm_2WO_9$) to $t = 0.978$ ($t = 0.977$) for $Ba_3Lu_2MoO_9$ ($Ba_3Lu_2WO_9$). This trend is in accordance with the variation of the β value against the Ln^{3+} ionic radius shown in Fig. 3. The β value increases from 90° with the increasing Ln^{3+} ionic radius, which means that the distortion from cubic symmetry becomes larger.

Figure 3 shows that the lattice parameters for $Ba_3Ln_2MO_9$ increase monotonically with the Ln^{3+} ionic radius. However, the value of $Ba_3Tb_2WO_9$ deviates greatly from this trend. This result means that the Tb ion is in the tetravalent state. This conclusion is based on the fact that the ionic radius of the tetravalent ion is smaller than that of the trivalent ion; 0.76 Å for Tb^{4+} ion and 0.923 Å for Tb^{3+} ion.

Powder neutron diffraction measurements on $Ba_3Tb_2WO_9$ were performed in order to determine its detailed structure. The diffraction profile is shown in Fig. 4. The Rietveld analysis for the collected data indicates that $Ba_3Tb_2WO_9$ adopts an ordered perovskite structure, which is consistent with the X-ray diffraction measurements. The refined structural parameters are summarized in Table 3. Its crystal structure is illustrated in Fig. 5. The results of the Rietveld analysis indicate that

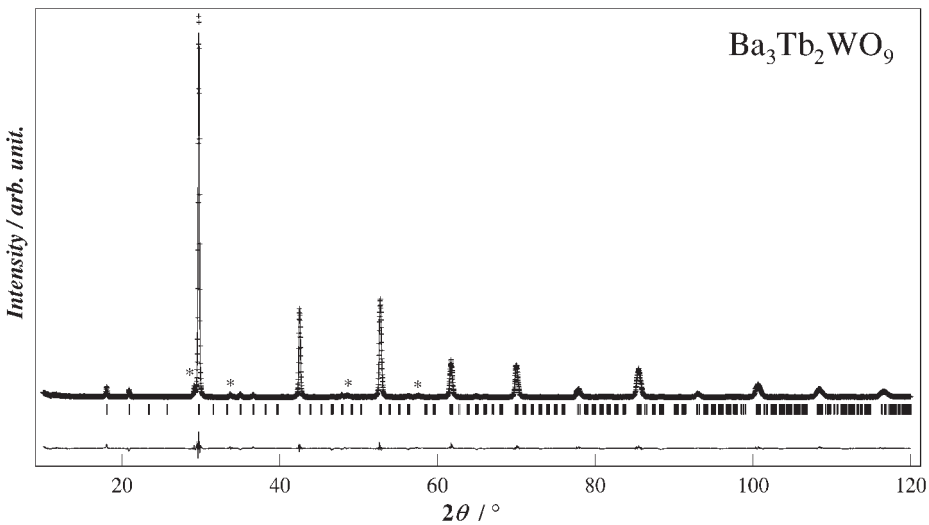

Fig. 2. X-ray diffraction profiles for $Ba_3Tb_2WO_9$. The calculated and observed diffraction profiles are shown on the top as a solid line and cross markers, respectively. The vertical marks show positions calculated from Bragg reflections. The bottom traces are plots of the difference between calculated and observed intensities. The asterisk in the profile corresponds to a diffraction peak for TbO_2 impurity.

Table 1. Lattice Parameters and *R* Factors of $Ba_3Ln_2MO_9$

Compounds	*a*	*b*	*c*	β	*V*	R_{wp}	R_I	R_F
$Ba_3Y_2MoO_9$	6.0120(2)	6.0126(4)	8.5390(2)	90.014(7)	308.66(2)	11.57	1.68	2.86
$Ba_3Sm_2MoO_9$	6.0930(5)	6.1244(4)	8.6333(5)	90.345(3)	322.15(4)	13.57	5.01	8.09
$Ba_3Eu_2MoO_9$	6.0814(4)	6.1044(7)	8.6118(9)	90.291(6)	319.70(5)	12.76	2.88	5.63
$Ba_3Gd_2MoO_9$	6.0680(4)	6.0900(4)	8.5893(5)	90.183(3)	317.41(3)	12.25	2.87	4.91
$Ba_3Dy_2MoO_9$	6.0311(6)	6.0323(5)	8.5515(5)	90.068(1)	311.11(5)	13.07	1.76	2.18
$Ba_3Ho_2MoO_9$	6.0149(3)	6.0150(3)	8.5472(3)	90.052(1)	309.23(2)	11.67	1.29	2.15
$Ba_3Er_2MoO_9$	5.9987(2)	5.9993(3)	8.5201(2)	90.041(1)	306.65(2)	11.04	1.00	1.91
$Ba_3Tm_2MoO_9$	5.9860(2)	5.9867(2)	8.4918(2)	90.028(1)	304.31(2)	9.91	1.34	2.65
$Ba_3Yb_2MoO_9$	5.9746(3)	5.9749(1)	8.4659(2)	90.011(8)	302.21(2)	11.22	1.13	1.86
$Ba_3Lu_2MoO_9$	4.2213(3)	—	—	—	75.22(8)	13.89	1.27	1.14
$Ba_3Y_2WO_9$	6.0054(6)	6.0125(3)	8.5288(6)	90.005(2)	307.96(4)	11.33	2.49	1.57
$Ba_3Sm_2WO_9$	6.0881(1)	6.1250(6)	8.6304(9)	90.029(6)	321.82(8)	14.49	2.48	1.73
$Ba_3Eu_2WO_9$	6.0664(9)	6.0951(4)	8.6028(6)	90.022(5)	316.15(5)	13.61	2.53	1.81
$Ba_3Gd_2WO_9$	6.0488(4)	6.0695(4)	8.5783(5)	90.012(7)	314.94(8)	12.03	1.77	1.19
$Ba_3Tb_2WO_9$	6.0070(7)	6.0131(6)	8.4931(12)	90.173(9)	306.77(6)	11.00	1.68	1.29
$Ba_3Dy_2WO_9$	6.0189(7)	6.0253(8)	8.5562(6)	90.007(5)	310.30(5)	11.79	1.88	1.49
$Ba_3Ho_2WO_9$	6.0029(3)	6.0115(2)	8.5289(4)	90.006(4)	307.78(2)	10.71	1.27	1.58
$Ba_3Er_2WO_9$	5.9910(4)	5.9995(2)	8.5018(4)	90.005(5)	305.58(3)	11.36	1.15	1.35
$Ba_3Tm_2WO_9$	5.9850(8)	5.9854(2)	8.4736(4)	90.004(8)	303.55(4)	9.78	1.02	1.03
$Ba_3Yb_2WO_9$	5.9762(2)	5.9773(8)	8.4499(3)	90.003(8)	301.84(4)	9.34	0.94	0.74
$Ba_3Lu_2WO_9$	5.9614(3)	5.9616(3)	8.4379(2)	90.003(3)	299.88(2)	9.79	1.09	0.76

$R_{wp} = [\sum w(|F(obs)| - |F(cal)|)^2 / \sum w|F(obs)|^2]^{1/2}$, $R_I = \sum |I_k(obs) - I_k(cal)| / \sum I_k(obs)$, and $R_F = \sum |[I_k(obs)]^{1/2} - [I_k(cal)]^{1/2}| / \sum [I_k(obs)]^{1/2}$.

Table 2. Structure Parameters for $Ba_3Lu_2MoO_9$[a)] and $Ba_3Ho_2MoO_9$[b)]

Atom	Site	Occupation	*x*	*y*	*z*	B/Å^2
(a) $Ba_3Lu_2MoO_9$						
Ba	1b	1.0	0.5	0.5	0.5	0.88(3)
Lu	1a	0.667	0	0	0	0.35(2)
Mo	1a	0.333	0	0	0	0.35(2)
O	3d	1.0	0.5	0	0	2.87(2)
(b) $Ba_3Ho_2MoO_9$						
Ba	4e	1.0	0	0.500(3)	0.25	0.81(3)
Lu	4a	0.667	0	0	0	0.36(3)
Mo	4a	0.333	0	0	0	0.36(3)
O1	4e	1.0	0	0.001(5)	0.25	3.11(2)
O_2	8f	1.0	0.232(6)	0.713(4)	0.003(1)	3.11(2)

a) Space group $Pm\bar{3}m$, lattice parameter: $a = 4.2213(3)$ Å, $R_{wp} = 13.89$ (%), $R_I = 1.27$ (%), and $R_F = 1.14$ (%). b) Space group $I2/c$, lattice parameter: $a = 6.0149(3)$ Å, $b = 6.0150(3)$ Å, $c = 8.5472(3)$ Å, $\beta = 90.052(1)^\circ$, $R_{wp} = 11.67$ (%), $R_I = 1.29$ (%), and $R_F = 2.15$ (%).

Table 3. Structure Parameters for $Ba_3Tb_2WO_9$[a)]

Atom	Site	Occupation	*x*	*y*	*z*	B/Å^2
Ba	4e	1.0	0.520(1)	0.503(4)	0.247(1)	0.69(6)
Tb(1)	2d	1.0	0	1/2	0	0.72(1)
Tb(2)	2c	0.333	1/2	0	0	0.72(1)
W	2c	0.667	1/2	0	0	0.72(1)
O(1)	4e	1.0	0.235(3)	0.233(2)	−0.022(2)	1.86(4)
O(2)	4e	1.0	0.241(3)	0.777(2)	−0.018(2)	1.86(4)
O(3)	4e	1.0	0.479(1)	−0.004(4)	0.231(1)	1.86(4)

a) Space group $P2_1/n$, lattice parameter: $a = 6.0059(4)$ Å, $b = 6.0134(3)$ Å, $c = 8.4931(7)$ Å, $\beta = 90.173(9)^\circ$, $R_{wp} = 4.11$ (%), $R_I = 4.41$ (%), and $R_F = 1.37$ (%).

$Ba_3Tb_2WO_9$ is actually a 1:1 ordered compound, i.e., one of the B sites is fully occupied by Tb, whereas the other contains 2/3W and 1/3Tb in a random distribution. The Tb and W ions in the $Ba_3Tb_2WO_9$ compound are alternatively arranged between Tb and (1/3Tb + 2/3W), and form a rock salt sublattice. Therefore, this compound should be described as $Ba_2Tb(Tb_{1/3}W_{2/3})O_6$.

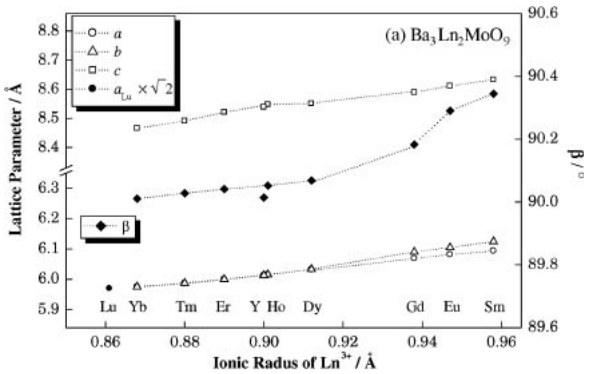

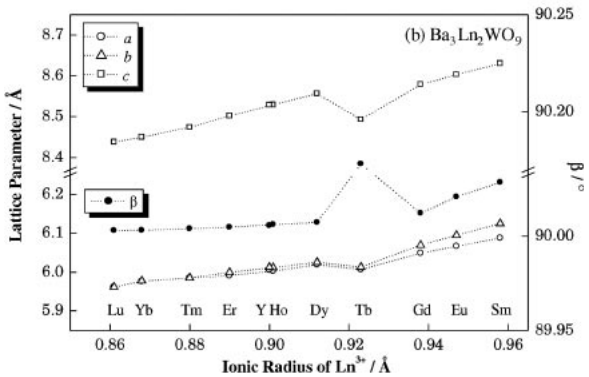

Fig. 3. The variation of lattice parameters with ionic radius of Ln^{3+} for (a) $Ba_3Ln_2MoO_9$ (Ln = Y, Sm–Gd, Dy–Lu) and (b) $Ba_3Ln_2WO_9$ (Ln = Y, Sm–Lu).

Magnetic Susceptibilities. Figure 6 shows the temperature dependence of the inverse magnetic susceptibilities for $Ba_3Ln_2MO_9$ (Ln = Sm–Yb, M = Mo and W). The Mo^{6+} and W^{6+} ions are both nonmagnetic, hence only the Ln^{3+} ions contribute to the magnetic properties of $Ba_3Ln_2MO_9$. These compounds are paramagnetic down to 1.8 K. The susceptibilities were fitted to the Curie–Weiss law over the entire temperature range for $Ba_3Gd_2MO_9$, or in higher temperature ranges (above 50 K for Ln = Tb–Tm compounds, above 150 K for $Ba_3Yb_2MO_9$). The determined effective magnetic moments and Weiss constants are listed in Table 4. The values of the effective magnetic moments are consistent with the free ion values, assuming that $\Delta E \gg k_B T$, where ΔE is the energy difference between the ground and excited states of the electronic multiplet. The value of the effective magnetic moment for $Ba_3Tb_2WO_9$ (8.94(4) μ_B) is smaller than the free ion value of the Tb^{3+} (9.72 μ_B). This indicates that the Tb ion is in the

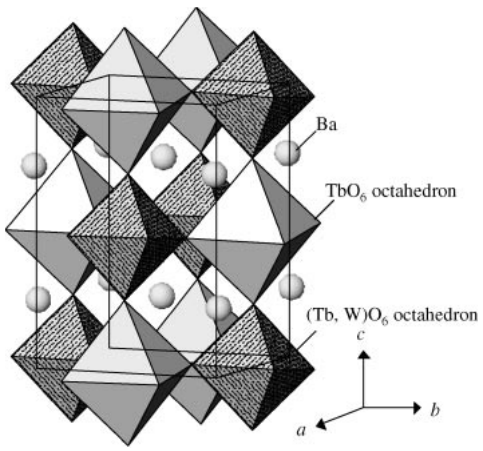

Fig. 5. The crystal structure of $Ba_3Tb_2WO_9$.

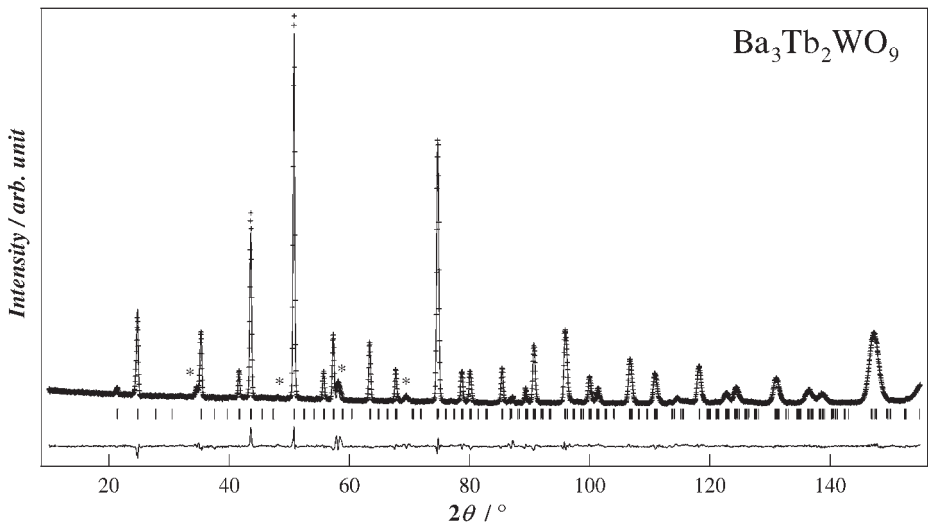

Fig. 4. Neutron diffraction profile for $Ba_3Tb_2WO_9$ at room temperature. The calculated and observed diffraction profiles are shown on the top as a solid line and cross markers, respectively. The vertical marks show positions calculated from Bragg reflections. The bottom traces are plots of the difference between calculated and observed intensities. The asterisk in the profile corresponds to a diffraction peak for TbO_2 impurity.

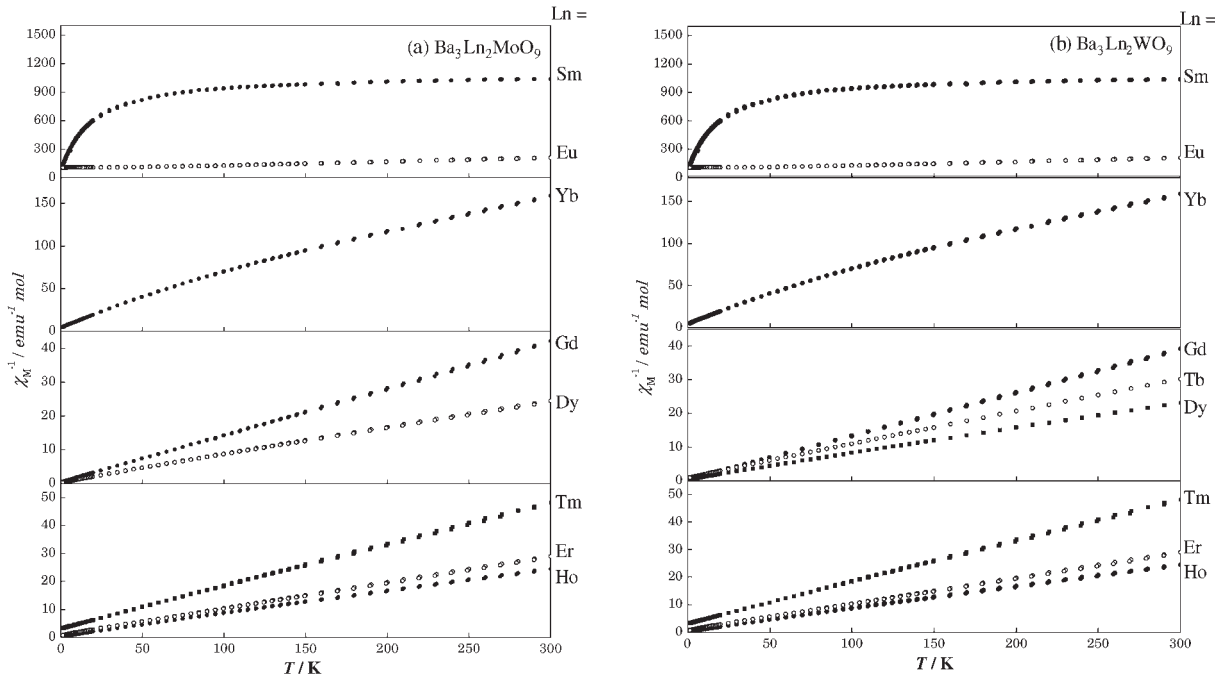

Fig. 6. Temperature dependence of the inverse magnetic susceptibilities of (a) $Ba_3Ln_2MoO_9$ (Ln = Sm–Gd, Dy–Yb) and (b) $Ba_3Ln_2WO_9$ (Ln = Sm–Yb).

Table 4. Calculated Magnetic Moments for Ln^{3+} (μ_{calc}), Experimental Magnetic Moments of Ln^{3+} (μ_{exp}), and Weiss Constants (Θ) for $Ba_3Ln_2MO_9$

Compounds	μ_{calc}/μ_B	μ_{exp}/μ_B	Θ/K
$Ba_3Gd_2MoO_9$	7.94	7.86(3)	−1.63(6)
$Ba_3Dy_2MoO_9$	10.63	10.17(6)	−11.94(8)
$Ba_3Ho_2MoO_9$	10.58	10.28(4)	−13.73(3)
$Ba_3Er_2MoO_9$	9.59	9.49(4)	−12.75(4)
$Ba_3Tm_2MoO_9$	7.55	7.44(4)	−25.2(1)
$Ba_3Yb_2MoO_9$	4.54	4.36(1)	−45.6(1)
$Ba_3Gd_2WO_9$	7.94	7.85(2)	−1.51(7)
$Ba_3Tb_2WO_9$	8.96[a)]	8.94(4)	−9.84(9)
$Ba_3Dy_2WO_9$	10.63	10.27(1)	−8.85(2)
$Ba_3Ho_2WO_9$	10.58	10.51(4)	−9.36(0)
$Ba_3Er_2WO_9$	9.59	9.48(2)	−8.82(9)
$Ba_3Tm_2WO_9$	7.55	7.56(8)	−25.3(4)
$Ba_3Yb_2WO_9$	4.54	4.46(2)	−53.0(1)

a) As discussed in the text, the ionic species in the $Ba_3Tb_2WO_9$ are $Ba^{2+}{}_3Tb^{3+}Tb^{4+}W^{5+}O^{2-}{}_9$. Therefore, the effective magnetic moment per mole of $Ba_3Tb_2WO_9$ is calculated to be $\sqrt{\mu_{Tb^{3+}}{}^2 + \mu_{Tb^{4+}}{}^2 + \mu_{W^{5+}}{}^2} = \sqrt{9.72^2 + 7.94^2 + 1.73^2} = 12.67\ \mu_B$. For comparison with the moments of other $Ba_3Ln_2MO_9$ compounds, the value of μ_{calc} for $Ba_3Tb_2WO_9$ is calculated to be $12.67/\sqrt{2} = 8.96\ \mu_B$ (per Tb).

mixed valence state (+3, +4), which is consistent with the above-mentioned arguments on the lattice parameter anomaly. Since the magnetic moment for the Tb^{4+} ion is 7.94 μ_B, the ratio of the Tb^{3+} and Tb^{4+} ions is estimated to be 1:1. In this case, the W ion is reduced to the pentavalent state to preserve charge neutrality in the solid (also see the note in Table 4). All of the Weiss constants are negative. This fact may indicate the existence of a Ln^{3+}–Ln^{3+} antiferromagnetic interaction. Due to the effect of the crystal field splitting, the magnetic susceptibilities of some compounds depart from the Curie–Weiss law at lower temperatures. For the case of the Tm and Yb compounds, their departure from the Curie–Weiss law occurs at relatively high temperatures,[11,12] which results in the large negative Weiss constants.

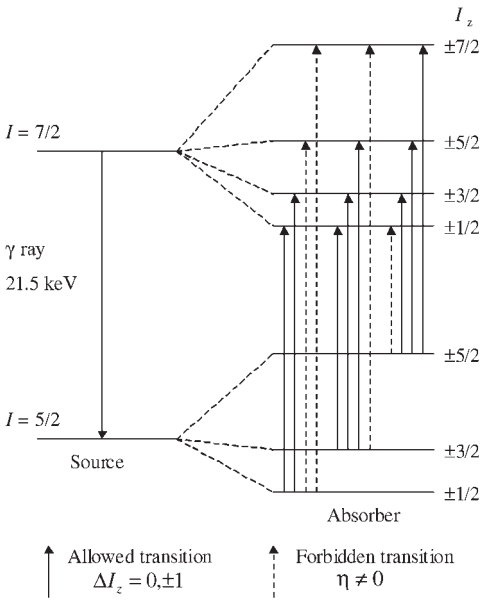

Fig. 7. The 12 possible transitions by a quadrupole interaction of ^{151}Eu nucleus.

^{151}Eu Mössbauer Spectra. ^{151}Eu Mössbauer spectra for $Ba_3Eu_2MoO_9$ and $Ba_3Eu_2WO_9$ measured at room temperature are shown in Fig. 7. Because of the low symmetry of the euro-

pium site in $Ba_3Eu_2MoO_9$ and $Ba_3Eu_2WO_9$ (point symmetry: $\bar{1}$), an electric field gradient tensor should exist at this site. The quadrupole Hamiltonian is given by:

$$H_{\text{quad}} = \frac{e^2qQ}{4I(2I-1)}[3I_z^2 - I(I+1) + \eta(I_x^2 - I_y^2)] \qquad (1)$$

where Q is the quadrupole moment, I is the nuclear spin, $eq = V_{zz}$, and $\eta = (V_{xx} - V_{yy})/V_{zz}$ (V_{ii} is the electric field gradient tensor). The asymmetry parameter η is not equal to zero because the symmetry at the Eu site is not axially symmetric. Then, the 12 possible transitions (eight allowed transitions and four forbidden transitions) due to quadrupole interactions were taken into account. Figure 7 shows the 12 possible transitions by quadrupole interactions of the ^{151}Eu nucleus. The observed spectra were fitted with the sum of these Lorenzian lines. In order to derive these Lorenzian equations, the results by Shenoy and Dunlap[13] were used, and the ratio of the excited and ground state quadrupole moments ($R_Q = Q_e/Q_g$) was taken to be 1.312.[14] Therefore, the parameters that should be fitted are the isomer shift (δ), the quadrupole coupling constant ($eV_{zz}Q_g$), the asymmetry parameter (η) and two common parameters for 12 Lorenzians, i.e., linewidth (Γ) and peak intensity (I_0).

The calculated spectra are shown in Fig. 8, and the obtained fitting parameters are listed in Table 5. The isomer shifts are 0.473 mm s^{-1} for $Ba_3Eu_2MoO_9$ and 1.479 mm s^{-1} for $Ba_3Eu_2WO_9$, which confirms that the europium ions are not in the divalent state, but in the trivalent state, because large negative isomer shifts (~ -12 mm s^{-1}) are observed for the Eu^{2+} ions.[15] The quadrupole coupling constants 4.3 and 6.3 mm s^{-1} and asymmetry parameters 0.94 and 0.67 mm s^{-1} show the existence of an electric field gradient at the Eu nuclei. The sign of $eV_{zz}Q_g$ is positive in this case, which is the same result as those for other perovskite-type compounds measured at room temperature.[3,16]

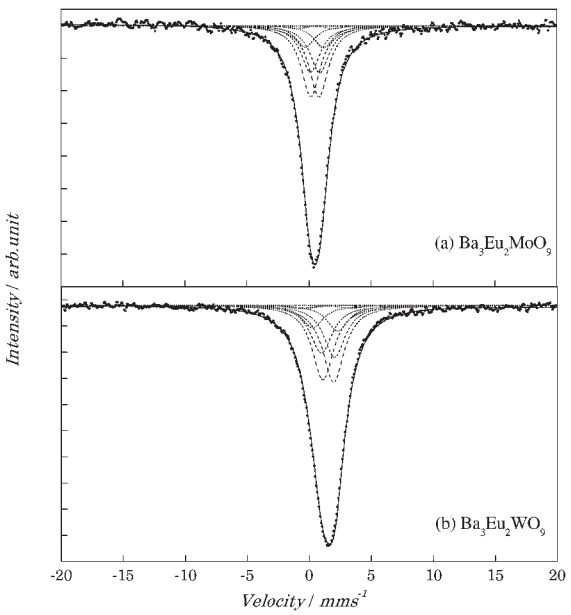

Fig. 8. ^{151}Eu Mössbauer spectra of (a) $Ba_3Eu_2MoO_9$ and (b) $Ba_3Eu_2WO_9$ measured at room temperature.

Table 5. ^{151}Eu Mössbauer Spectrum Parameters for $Ba_3Eu_2MoO_9$ and $Ba_3Eu_2WO_9$ at Room Temperature

	δ/mm s^{-1}	$eV_{zz}Q_g$/mm s^{-1}	η	Γ/mm s^{-1}	I_o/%
$Ba_3Eu_2MoO_9$	0.473(5)	4.3(1)	0.94(6)	1.88(3)	8.9(1)
$Ba_3Eu_2WO_9$	1.479(4)	6.3(1)	0.67(3)	2.10(2)	11.9(8)

Summary

Perovskite-type oxides $Ba_3Ln_2MO_9$ (Ln = Y, Sm–Gd, Dy–Lu for M = Mo; Ln = Y, Sm–Lu for M = W) were prepared. The Rietveld analyses of the X-ray diffraction data show that the Ln and M cations are disordered at the B site of the perovskites except for $Ba_3Tb_2WO_9$. Their structures are refined by applying the space group $Pm\bar{3}m$ for the $Ba_3Lu_2MoO_9$ and $I2/c$ for the other compounds. $Ba_3Tb_2WO_9$ has an ordered perovskite structure and is monoclinic with space group $P2_1/n$. The result of the Rietveld analysis indicates that $Ba_3Tb_2WO_9$ is actually a 1:1 ordered compound, i.e., one of the B sites is fully occupied by Tb, whereas the other contains 2/3W and 1/3Tb with a random distribution.

The Magnetic susceptibility measurements show that all the compounds are paramagnetic down to 1.8 K. The Tb ions of $Ba_3Tb_2WO_9$ are in mixed valence states (+3, +4). Through ^{151}Eu Mössbauer measurements for $Ba_3Eu_2MoO_9$ and $Ba_3Eu_2WO_9$, it was found that the Eu ion is in the trivalent state, and the six oxygens coordinated around the Eu site are distorted from octahedral symmetry.

The present study was supported by the Japan Securities Scholarship Foundation.

References

1 J. B. Goodenough and J. M. Longo, "Landolt-Börnstein," New Series, Vol. III/4a, Springer, Berlin (1970).

2 M. T. Anderson, K. B. Greenwood, G. A. Taylor, and K. R. Poeppelmeier, *Prog. Solid State Chem.*, **22**, 197 (1993).

3 K. Henmi, Y. Hinatsu, and N. Masaki, *J. Solid State Chem.*, **148**, 353 (1999).

4 Y. Doi and Y. Hinatsu, *J. Phys. Condens. Mater.*, **13**, 4191 (2001).

5 Y. Izumiyama, Y. Doi, M. Wakeshima, Y. Hinatsu, Y. Shimojo, and Y. Morii, *J. Phys. Condens. Mater.*, **13**, 1303 (2001).

6 M. Wakeshima, D. Harada, Y. Hinatsu, and N. Masaki, *J. Solid State Chem.*, **147**, 618 (1999).

7 Y. Doi and Y. Hinatsu, *J. Mater. Chem.*, **12**, 1792 (2002).

8 F. Izumi and T. Ikeda, *Mater. Sci. Forum*, **321–324**, 198 (2000).

9 V. Nassif, R. E. Carbonio, and J. A. Alonso, *J. Solid State Chem.*, **146**, 266 (1999).

10 P. D. Battle, T. C. Gibb, and C. W. Jones, *J. Solid State Chem.*, **78**, 281 (1989).

11 A. Abragam and B. Bleaney, "Electron Paramagnetic Resonance of Transition Ions," Oxford Univ. Press, London (1970), Chap. 5.

12 N. Taira and Y. Hinatsu, *J. Solid State Chem.*, **150**, 31 (2000).

13 G. K. Shenoy and B. D. Dunlap, *Nucl. Instrum. Mathods*, **71**, 285 (1969).

14 J. G. Stevens, "Handbook of Spectroscopy," ed by J. W. Robinson, Chemical Rubber Company, Boca Raton, FL (1981), Vol. III, p. 464.

15 M. Wakeshima, Y. Doi, Y. Hinatsu, and N. Masaki, *J. Solid State Chem.*, **157**, 117 (2001).

16 M. Wakeshima, D. Harada, and Y. Hinatsu, *J. Mater. Chem.*, **10**, 419 (2000).